

KINETICS OF METHANE HYDRATE FORMATION IN PURE WATER AND INHIBITOR CONTAINING SYSTEMS

Tian-Min Guo and Jun-Hong Qiu
High Pressure Fluid Phase Behavior & Property Research Laboratory
University of Petroleum
Beijing, P.R. China 100083

Keywords: Kinetics, Methane hydrate formation, Brines

INTRODUCTION

The discovery of huge deposits of methane hydrate *in situ* (a possible energy source in the future), the production problems associated with the offshore oil/gas exploitation/transportation, and the new applications of hydrate technology have renewed interest in hydrate research in the past decade.

The two basic problems to be studied are the hydrate equilibrium thermodynamics and the hydrate formation/dissociation kinetics. Most of the papers published previously have been related to the former topic, a number of engineering applicable thermodynamic models has been developed, including recent models for salt-containing systems (Zuo et al., 1996; etc.). Compared to hydrate equilibrium thermodynamics, our knowledge on the kinetics of hydrate formation are far from mature. Due to the complexity of the dynamic process of hydrate formation, and the lack of consistent experimental data, a generalized kinetic model is not yet available. Since knowledge of the kinetics of hydrate formation is of critical importance in the transportation pipeline design, effective utilization of the methane hydrate resource *in situ*, and the various applications of hydrate technology, it has received increasing attention in recent years. Comprehensive reviews on the progress are available (Sloan, 1990; Makogon, 1981; Englezos, 1993; and Qiu and Guo, 1995).

The major objectives of this work are: (1) Measure the kinetic data of methane hydrate formation in the presence of pure water, brines containing single salt and mixed salts, and aqueous solutions of ethylene glycol (EG)/(salt + EG). (2) Develop a new kinetic model of hydrate formation for the methane + pure water systems based on a four-step formation mechanism and reaction kinetics approach. (3) Explore the feasibility of extending the proposed kinetic model to salt(s) and EG containing systems.

EXPERIMENTAL SECTION

Apparatus. It is well known that the specific equipment used in the study of hydrate formation kinetics has significant influence on the experimental results. There are basically two types of equipment, fixed boundary type and turbulent boundary type. The former is more suitable for simulating the hydrate formation/dissociation *in situ*, and the latter is closer to the conditions in the transportation pipelines and natural gas processing equipment. The apparatus used in this work belongs to the latter type. The schematic diagram of the experimental system is shown in Fig. 1, and the major parts are briefly described as follows:

Transparent sapphire cell: The 2.5 cm i.d. sapphire cell was purchased from the DB Robinson Design & Manufacturing Ltd. (Canada), the total volume and the effective volume (excluding the piston and stirrer volume) are 78 and 59 mL, respectively. The working volume of the cell can be adjusted by a floating piston driven by a positive displacement pump. The maximum working pressure and temperature are 20 MPa and 423 K, respectively.

Air bath: The air bath was manufactured by Shanghai Instruments Corp., the working temperature range is 263 ~ 373 K and can be controlled to within ± 0.2 K by a digital programmable temperature controller.

Agitation system: The agitation system consists of a magnetic stirrer coupled with a permanent magnet mounted outside of the cell. A variable speed DC motor equipped with an rpm-controller provides up and down reciprocating motion of the magnet.

Pressure measurement: The pressure in the cell was measured through pressure transducer and pressure gauge simultaneously. A differential pressure transducer (Honeywell Inc.) was connected with the data acquisition system. The precision of the DP transducer at the working span (0 ~ 10 MPa) is ± 0.1 %. A 0 ~ 25 MPa Heise pressure gauge was also installed for taking parallel pressure readings. The pressure measurement system was calibrated against a Ruska standard dead-weight gauge, and the precision of the pressure measurements is estimated at ± 0.015 MPa.

Experimental Procedure. The kinetics of hydrate formation can be studied in two modes: the constant temperature-constant pressure mode and the constant temperature-constant volume mode. In the former mode, to maintain constant system pressure, the hydrate former gas consumed in the hydrate formation process is continuously supplemented from outside. In the latter mode, the system is closed, with its volume kept constant, and the system pressure is lowered gradually in the hydrate formation process. The latter mode was applied in this study.

Prior to performing the experiment, the floating piston was lowered to the bottom of the sapphire cell and its position was unchanged during the measuring process. About 12 mL liquid sample was charged into the evacuated sapphire cell. When the system temperature stabilized at the preset value, methane was introduced into the cell until the pressure was raised to about 4.0 MPa. The gas was then discharged to eliminate the trace amounts of residual air in the cell. Methane was again charged until the preset initial

system pressure was attained, then the DC motor to actuate the magnetic stirrer was started with the stirrer was moving up and down at a rate of four strokes per minute. The system temperature and the change of system pressure were recorded through the data acquisition system every 30 seconds, and displayed on the monitor screen.

Experiments Performed. The systems studied and the corresponding operating conditions are summarized in Table 1. A total of 30 sets of kinetic data were measured for the following systems: methane + water, methane + water + salt(s), methane + water + EG, and methane + water + salt + EG.

Experimental Results. A typical pressure vs. time ($P \sim t$) curve measured for the methane hydrate formation process is shown in Fig. 2. The curve can be roughly divided into three zones. The first zone (from t_0 to t_s) is called the "gas dissolution zone", P_s stands for the system pressure when saturation of the dissolved gas is established. The second zone (from t_s to t_r) is called the "nucleation zone", system pressure remains nearly at constant in this zone. The time interval from t_0 to t_r is the so called induction period. The third zone, from t_r to t_d , is called the "crystal growth zone", in this zone the system pressure falls gradually from P_r to P_d and remains stabilized after time t_d . The three zones are divided rather arbitrarily, as in fact, nucleation could proceed simultaneously with the gas dissolution process. The relative time distribution of the three zones in the 30 experiments performed are also listed in Table 1. The detailed $P \sim t$ data for typical experiments are given in Table 3 and Figs. 3 ~ 5 along with the calculated results which are discussed below.

Analysis of the Experimental Results. From Table 1, it can be seen that the time interval of the gas dissolution period is, in general, 1 ~ 2 hours, however, the time interval of nucleation period differs appreciably for the experiments performed, from ~ 25 minutes (E04, E08, and E25) to ~ 5 hours (E16), and for some experiments (E01 and E20) no crystal nucleus was formed even after 10 hours. Since during the nucleation period, the liquid phase is in the metastable state, the nucleation process is sensitive to very small perturbations to the system. This caused difficulty in obtaining repeatable results even when the experiments were run under identical temperature and initial pressure conditions (E09a ~ E09c). The time period for crystal growth also differed significantly for experiments run under different operating conditions, from 80 minutes (E04) to more than 5 hours (E28).

Under the same operating temperatures, the initial pressure has little effect on the time interval of gas dissolution period (E01 ~ E04 and E05 ~ E09), however, its influence on the nucleation period is significant. In general, the lower the initial pressure, the longer of the nucleation period. Similar initial pressure effect was observed in the crystal growth period (E02 ~ E04 and E07 ~ E09).

The temperature effect on the time interval of gas dissolution and nucleation periods (under same initial pressure) is, in general, the higher the temperature, the longer the time period (E10 and E12, E08 and E11). The effect increases with the lowering of the initial pressure. Significant temperature effect was also observed in the crystal growth period; the time interval increase almost linearly with the increase of temperature, however, the temperature effect seemed not as sensitive to the initial pressure in this period.

The effects of inhibitors (salt/ethylene glycol) on the hydrate formation process are quite complex. When the concentration of the inhibitor is less than 1.0 mass%, the effect of concentration is not obvious on the time distribution of the three periods (E13 and E14, E17 and E18, E21 and E22).

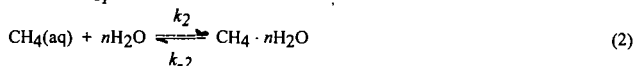
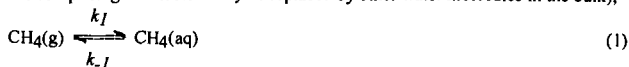
For concentrations greater than 1.0 mass%, the time interval of gas dissolution period is little effected by the inhibitor concentration, however, the concentration has significant effect on the time interval of nucleation period, the higher the concentration the longer the time interval (E15 and E16, E19 and E20, E23 and E24, E26 and E28). The order of inhibition effect is as follows (when concentration of inhibitor > 1.0 mass%): EG > NaHCO₃ > NaCl > (NaCl + NaHCO₃) > (NaHCO₃ + EG) > (NaCl + EG).

An interesting phenomenon observed in the experiments is that when the concentration of inhibitor is less than 1.0 mass% (E13, E14, E17, E18 and E25), the induction time (gas dissolution period + nucleation period) is significantly shorter as compared with the methane + pure water systems (run under similar temperature and initial pressure conditions). It is in consistency with the observation of Yousif et al. (1994), that the hydrate formation could be enhanced at low inhibitor concentration.

MECHANISM OF METHANE HYDRATE FORMATION

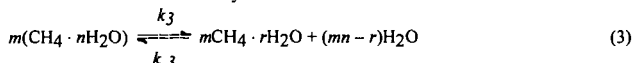
In this work, the mechanism of methane hydrate formation in pure water was described by the following four steps.

Step 1: A portion of the methane molecules in the gas phase dissolve into the aqueous phase, and the dissolved methane molecules are clathrated by n water molecules to form a metastable cluster (i.e. the water molecules comprising the clusters may be replaced by other water molecules in the bulk),



Following Long and Sloan (1993), the coordination number n was taken as 20. Since the structure of this labile cluster is similar to the 5^{12} hydrate cavity (Christiansen and Sloan, 1994), we assume their size is also similar, i.e. ~ 0.5 nm.

Step 2: The link of clusters to form a crystal unit.



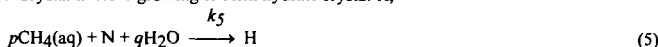
It has been well established that methane forms structure I hydrate, the structure I hydrate crystal unit cell contains 46 water molecules, and consists of two 5^{12} and six $5^{12}6^2$ crystal cavities. The maximum number of methane molecules per unit cell is 8. Assume the crystal unit in Eq. (3), $m\text{CH}_4 \cdot r\text{H}_2\text{O}$, is an ideal crystal unit cell (with its cavities fully occupied), thus $m = 8$, and $r = 46$. It is also assumed that the size of the crystal unit cell $m\text{CH}_4 \cdot r\text{H}_2\text{O}$ is the same as the crystal unit cell of structure I hydrate, and is thus taken as 1.2 nm (van der Waals and Platteeuw, 1959). Since the size of the crystal unit is smaller than the critical size, some of the crystal units could be dissociated back to individual labile molecular clusters, and the others will be further linked to form a stable *crystal nucleus*, its size exceeding a certain critical size.

Step 3: Crystal units linked to form crystal nucleus N,



Englezos et al. (1987) proposed an equation for calculating the critical size of hydrate crystal nucleus. Based on the proposed equation, Natarajan et al. (1994) calculated the critical size of the methane hydrate crystal nucleus to be approximately 10–30 nm. That means, about 8–25 unit cells with a size of 1.2 nm are required to form a crystal nucleus of the critical size, i.e. $l = 8\text{--}25$. Thus, approximately 64–200 methane molecules and 368–1150 water molecules are required to form a crystal nucleus of critical size.

Step 4: Crystal nucleus growing to form hydrate crystal H,



During the crystal nucleus growing period, hydrate crystals H with different sizes could be formed. Graauw and Rutten (1970) has measured the size distribution of propane hydrate crystals (structure II) in a continuous stirred tank crystallizer, the results showed that the crystal size is within 10–35 μm , the average being about 20 μm . Bylov and Rasmussen (1996), Monfort and Nzihou (1993) have also studied the crystal size distribution. Based on the size distribution data available, we can conclude that the size of the methane hydrate crystal is at least three times in magnitude larger than the size of the critical crystal nucleus. The magnitude of p and q in Eq. (5) should be 10^5 and 10^6 , respectively.

KINETIC EQUATIONS

For simplifying the derivation of the rate equations involved in the hydrate formation process, the following assumptions were made:

(1) The rate of concentration change of each component (r_i) in the reactions shown in Eqs. (1) to (5) can be expressed in the following polynomial form,

$$r_i = -\frac{dC_i}{dt} = kC_i^\alpha C_j^\beta \dots \quad (6)$$

where C_i and C_j represent the concentration (mol/L) of components i and j , α and β denote the order of concentration change.

(2) The order of concentration change is unity for all components ($\alpha = \beta = 1.0$).

(3) The water content in the aqueous phase is constant during the hydrate formation process.

(4) The volume of gas phase and liquid phase remain unchanged during the hydrate formation process.

Based on the above assumptions, the following rate equations can be derived:

$$\frac{dC_G}{dt} = -k_1 C_G + k_{-1} C_A \quad (7)$$

$$\frac{dC_A}{dt} = k_1 C_G - k_{-1} C_A - k_2 C_A + k_{-2} C_B - pk_5 C_A C_N \quad (8)$$

$$\frac{dC_B}{dt} = k_2 C_A - k_{-2} C_B - mk_3 C_B + mk_{-3} C_D \quad (9)$$

$$\frac{dC_D}{dt} = k_3 C_B - k_{-3} C_D - lk_4 C_D \quad (10)$$

$$\frac{dC_N}{dt} = k_4 C_D - k_5 C_A C_N \quad (11)$$

$$\frac{dC_H}{dt} = k_5 C_A C_N \quad (12)$$

where C_G stands for the apparent mole concentration of methane in the gas phase (mole of methane in gas phase per liter of liquid phase), C_A , C_B , C_D , C_N and C_H denote the concentrations (mol/L) of $\text{CH}_4(\text{aq})$, $\text{CH}_4 \cdot n\text{H}_2\text{O}$, $m\text{CH}_4 \cdot r\text{H}_2\text{O}$, N and H, respectively. Based on assumption (3), the concentration of water in the liquid phase does not appear in the rate equations. At initial conditions: $t = 0$, $C_G = C_G^0$, $C_A = C_B = C_D = C_N = C_H = 0$, from mass balance of methane we have:

$$C_G^0 = C_G + C_A + C_B + mC_D + lmC_N + (p + lm)C_H \quad (13)$$

Since C_G , C_A , C_B , C_D , C_N and C_H are restrained by Eq. (13), only five of the above six concentration variables are independent. The concentration of the metastable molecular cluster C_B was chosen as a dependent variable. From Eq. (13) we have:

$$C_B = C_G^0 - C_G - C_A - mC_D - lmC_N - (p + lm)C_H \quad (14)$$

Eq. (9) can then be removed from the rate equation set. Substituting Eq. (14) into Eqs. (8) and (10) yields:

$$\frac{dC_A}{dt} = k_{-2}C_G^0 + (k_1 - k_{-2})C_G - (k_{-1} + k_2 + k_{-2})C_A - mk_{-2}C_D - lm_{k_{-2}}C_N - (p + lm)k_{-2}C_H - pk_5C_A C_N \quad (15)$$

$$\frac{dC_D}{dt} = k_3(C_G^0 - C_G) - k_3C_A - (mk_3 + k_{-3} + lk_4)C_D - lm_{k_3}C_N - (p + lm)k_3C_H \quad (16)$$

The initial conditions are changed to: $t = 0$, $C_G = C_G^0$, $C_A = C_D = C_N = C_H = 0$.

Eqs. (7), (11), (12), (15) and (16) coupled with the corresponding initial conditions constitute the mathematical model of the kinetic behavior of methane hydrate formation in pure water.

THE LEAST SQUARE ESTIMATION OF THE KINETIC PARAMETERS

In the rate equations established in the previous section, there are eight unknown parameters: k_1 , k_{-1} , k_2 , k_{-2} , k_3 , k_{-3} , k_4 and k_5 . As k_1 and k_{-1} are restrained by the following expression of equilibrium constant K_c (derivation is referred to the expanded manuscript):

$$K_c = \frac{k_1}{k_{-1}} = \frac{C_w^0 Z R T V_l}{C_w^0 Z R T V_l} \quad (17)$$

where C_w^0 , Z and H denote the initial water concentration, compressibility of methane and Henry's constant of methane, respectively. k_{-1} can be calculated through k_1 as follows:

$$k_{-1} = \frac{k_1}{K_c} = \frac{k_1 H V_g}{C_w^0 Z R T V_l} \quad (18)$$

Thus, only seven unknown parameters (k_1 , k_2 , k_{-2} , k_3 , k_{-3} , k_4 and k_5) in the kinetic equations needed to be determined.

The damped nonlinear least square method was used for parameter estimation, the details of the algorithm are also given in the expanded manuscript (which is available on request). The regressed parameter values for the methane + water systems are tabulated in Table 2, and a typical comparison between experimental and calculated $P \sim t$ data for Experiment E09b is shown in Fig. 3.

TEST ON THE PROPOSED KINETIC MODEL

Sensitivity on Initial Pressure. Experiments E01 ~ E04 were run under the same temperature (273.65 K) and different initial pressures. Tests were performed on the prediction of the $P \sim t$ data of E01 ~ E03 based on the parameter values determined from E04. The test results show that, in the gas dissolution zone the deviations between experimental and calculated gas phase pressure are in the range of $-0.11\% \sim -0.50\%$; in the nucleation zone, the maximum relative deviations are -0.37% for E02 and E03, and 0.74% for E01 (no hydrate finally formed); and in the hydrate growth zone, the maximum relative deviation is -0.29% for E02 and E03. Typical comparison between the experimental and predicted $P \sim t$ curves for E01 is shown in Fig. 4.

Experiments E05 ~ E09 were also run at the same temperature (274.15 K) and different initial pressures. The $P \sim t$ data of Experiments E08, E09b and E09c were predicted by using the parameter values determined from E07. In the gas dissolution zone, the measured and calculated gas phase pressures are close, the maximum relative deviation is 0.38% . In the nucleation zone, the maximum deviations are -0.059% for E08, and 0.54% for E09b and E09c. In the crystal growth zone, the maximum deviations for E08, E09b and E09c are 0.78% , 1.01% and 0.52% , respectively.

The test results indicate that although the kinetic data of hydrate formation depend on the initial pressure, the model parameters determined from a specific run are capable of predicting the $P \sim t$ data of runs carried out at different initial pressures (under same temperature) with good accuracy.

Prediction of the $P \sim t$ Data for Salt/EG Containing Systems. The prediction of the kinetic data of methane hydrate formation in brines and aqueous solution of EG are of particular interest in real production processes and has not been previously reported. It is well known that the presence of salt(s) and alcohol in the aqueous phase can inhibit the hydrate formation (similar to the freezing point depression), as the solubility of methane will be significantly lowered, and the physical properties (viscosity, density, diffusivity, interfacial tension, etc.) of the aqueous phase will in turn be significantly changed. As a preliminary attempt to extend the proposed kinetic model to the salt/ethylene glycol containing systems, we assumed the solubility of methane in the aqueous phase (expressed in terms of the Henry's constant of methane) is the critical factor affecting the inhibition of methane hydrate formation. The larger the Henry's constant, the greater the inhibition effect.

Among the eight parameters in the proposed kinetic model, k_{-1} is the only parameter related to Henry's constant, hence, the other model parameters determined from methane + pure water system can be applied directly to the salt/ethylene glycol containing systems. For illustration purposes, the $P \sim t$ data of methane hydrate formation in 5.0 mass% NaCl solution (Experiment E16) were predicted by using the kinetic parameters determined from Experiment E09b performed on methane + pure water system (E16 and E09b were run at the same temperature and initial pressure conditions). The Henry's constant of methane in the 5.0 mass% NaCl solution at 274.15 K was taken from Cramer (1984), $H = 3.642 \times 10^3$. The comparison between the predicted and experimental results is presented in Fig. 5. Fairly good prediction results were observed, the maximum deviations of the predicted gas phase pressure are -0.13 % in the gas dissolution zone, and 0.31 % in the nucleation and crystal growth zones.

CONCLUSIONS

- (1) The new kinetic model developed from a four-step hydrate formation mechanism and reaction kinetics approach is capable of describing the $P \sim t$ data measured in this work.
- (2) Under identical temperature condition, the kinetic parameters determined for a specific initial pressure can be applied to estimate the $P \sim t$ data run at other initial pressures (within the pressure range of this study), the maximum deviation is within 0.3%.
- (3) The kinetic model developed for methane + water systems can be extended to inhibitor containing systems by replacing the Henry's constant of methane in corresponding aqueous phase.
- (4) As the dynamic behavior of hydrate formation is strongly dependent on the type of equipment and agitation intensity, the kinetic data measured in this work can only be considered as typical for a mildly agitated non-flowing system.

ACKNOWLEDGMENT

Financial support received from the China National Science Foundation, Postdoctoral Research Foundation and the China National Petroleum & Natural Gas Corporation are gratefully acknowledged.

REFERENCES

- M. Bylov and P. Rasmussen, A new technique for measuring gas hydrate kinetics, Proceedings of the 2nd International Conference on Natural Gas Hydrates, June 2-6, 1996, Toulouse, France, 259-266.
- R. L. Christiansen and E. D. Sloan, Mechanisms and kinetics of hydrate formation, Annals of the New York Academy of Sciences, Vol. 715 (1994) 283-305.
- S. D. Cramer, Solubility of methane in brines from 0 to 300 °C, Ind. Eng. Chem. Proc. Des. Dev., 23 (1984) 533-538.
- J. de Graauw and J. J. Rutten, The mechanism and the rate of hydrate formation, Proceedings 3rd Int. Symp. on Fresh Water from the Sea, 1970, Athens, 103-116.
- P. Englezos, N. Kalogerakis, P. D. Dholabhai and P. R. Bishnoi, Kinetics of formation of methane and ethane gas hydrates, Chem. Eng. Sci., 42 (1987) 2647-2658.
- P. Englezos, Clathrate hydrates, Ind. Eng. Chem. Res., 32 (1993) 1251-1274.
- J. Long and E. D. Sloan, Quantized water clusters around apolar molecules, J. Mol. Simul., 11 (1993) 145-161.
- Y. F. Makogon, Hydrates of Natural Gas (translated from Russian by W. J. Cieslewicz), PennWell, Tulsa, 1983.
- J. P. Monfort and A. Nzihou, Light scattering kinetics study of cyclopropane hydrate growth J. Crystal Growth, 128 (1994) 1182-1186.
- V. Natarajan, P. R. Bishnoi and N. Kalogerakis, Induction phenomena in gas hydrate nucleation, Chem. Eng. Sci., 49 (1994) 2075-2087.
- J.-H. Qiu and T.-M. Guo, Status of the kinetic studies on the hydrate formation/dissociation, J. Ind. & Eng. Chem. (China), 46 (1996) 741-756.
- P. Skovborg, H. J. Ng, P. Rasmussen and U. Mohn, Measurement of induction times for the formation of methane and ethane hydrates, Chem. Eng. Sci., 48 (1993) 445-453.
- E. D. Sloan, Clathrate Hydrates of Natural Gas, Marcel Dekker, New York, 1990.
- J. A. van der Waals and J. C. Platteeuw, Clathrate solutions, Adv. Chem. Phys., 2 (1959) 2-57.
- M. H. Yousif, R. B. Dorshow and D. B. Young, Testing of hydrate kinetic inhibitors using laser scattering technique, Annals of the New York Academy of Sciences, Vol. 715 (1994) 330-340.
- Y.-X. Zuo, S. Gommessen and T.-M. Guo, Equation of state based hydrate model for natural gas systems containing brine and polar inhibitor, Chinese J. Chem. Eng. (in English), 4 (1996) 189-202.

Table 1. Summary of the methane hydrate systems studied and the time distribution of three zones

Exp. No.	Aqueous phase*	Temp. (K)	Initial Press. (MPa)	Gas dissolution zone (min)	Nucleation zone (min)	Crystal growth zone (min)
E01	H ₂ O	273.65	4.47	100	645*	-
E02	H ₂ O	273.65	5.46	100	80	150
E03	H ₂ O	273.65	7.45	100	100	125
E04	H ₂ O	273.65	8.47	95	25	80
E05	H ₂ O	274.15	4.49	100	575*	-
E06	H ₂ O	274.15	5.10	105	510*	-
E07	H ₂ O	274.15	5.46	95	90	205
E08	H ₂ O	274.15	5.96	95	25	185
E09a	H ₂ O	274.15	6.46	105	195*	-
E09b	H ₂ O	274.15	6.46	105	105	160
E09c	H ₂ O	274.15	6.47	105	32	183
E10	H ₂ O	274.65	6.47	90	30	195
E11	H ₂ O	275.15	6.00	130	165	280
E12	H ₂ O	276.15	6.47	110	40	390
E13	NaCl (0.5)+H ₂ O	274.15	6.46	60	38	160
E14	NaCl (1.0)+H ₂ O	274.15	6.47	65	30	185
E15	NaCl (3.0)+H ₂ O	273.65	6.47	110	150*	-
E16	NaCl (5.0)+H ₂ O	274.15	6.45	110	325	150
E17	NaHCO ₃ (0.5)+H ₂ O	274.15	6.45	65	32	168
E18	NaHCO ₃ (1.0)+H ₂ O	274.15	6.46	65	30	200
E19a	NaHCO ₃ (3.0)+H ₂ O	274.15	6.47	115	210	195
E19b	NaHCO ₃ (3.0)+H ₂ O	274.15	6.48	115	200	200
E20	NaHCO ₃ (5.0)+H ₂ O	273.65	6.46	120	615*	-
E21	EG (0.5)+H ₂ O	274.15	6.47	110	340*	-
E22	EG (1.0)+H ₂ O	274.15	6.46	115	345*	-
E23	EG (5.0)+H ₂ O	273.65	6.47	115	25	185
E24	EG (10.0)+H ₂ O	273.65	6.47	120	505*	-
E25	NaCl (0.5)+ NaHCO ₃ (0.5)+H ₂ O	274.15	6.47	60	25	185
E26	NaCl (1.5)+ NaHCO ₃ (1.5)+H ₂ O	274.15	6.47	90	35	250
E27	NaCl (2.5)+ NaHCO ₃ (2.5)+H ₂ O	273.65	6.47	100	65	290
E28	NaCl (2.5)+ NaHCO ₃ (2.5)+H ₂ O	274.15	6.47	95	60	320
E29	NaCl (2.5)+ EG (2.5)+H ₂ O	273.65	6.47	90	55	235
E30	NaHCO ₃ (2.5) + EG (2.5)+H ₂ O	273.65	6.47	90	112	203

* Numbers in parentheses are mass percent of inhibitor; EG stands for ethylene glycol.

No hydrate crystal formed in this time period.

Table 2. Estimated kinetic parameter k_j values for various experiments on methane + water systems

Exp. No.	$k_1 \times 10^3$	$k_2 \times 10^2$	$k_{.2} \times 10$	$k_3 \times 10^3$	$k_{.3} \times 10^2$	$k_4 \times 10$	k_5
E02	33.99	135.1	45.37	0.3735	5.037	0.4297	6.626
E03	32.95	187.3	41.57	0.2669	8.527	0.1839	5.261
E04	19.46	12.13	28.48	1.470	5.386	4.097	10.93
E07	29.05	0.8026	6.543	6.374	9.195	10.94	4.976
E08	15.54	55.59	0.3661	0.01616	3.923	6.708	0.5876
E09b	14.15	0.03878	1.189	139.2	0.2266	0.7779	4.224
E09c	8.539	21.95	0.3699	0.03070	4.771	4.390	0.8824
E10	13.74	10.64	34.31	1.447	34.34	28.15	9.487
E11	21.28	0.9161	4.622	1.792	6.435	8.710	3.455
E12	10.22	94.46	3.016	0.02347	4.746	7.368	0.9024

Table 3. Comparison of the experimental and calculated gas phase pressure for the Experiments E09b and E16*

Experiment E09b				Experiment E16			
t (min)	P_{exp} (MPa)	P_{calc} (MPa)	Rel. Dev. (%)	t (min)	P_{exp} (MPa)	P_{calc} (MPa)	Rel. Dev. (%)
0.0	6.465	—	—	0.0	6.447	—	—
10.0	6.452	6.453	-0.018	15.0	6.430	6.431	-0.022
20.0	6.441	6.444	-0.040	30.0	6.417	6.422	-0.078
30.0	6.429	6.436	-0.110	40.0	6.412	6.418	-0.088
45.0	6.424	6.426	-0.034	55.0	6.405	6.414	-0.13
60.0	6.421	6.419	+0.036	75.0	6.401	6.410	-0.14
75.0	6.412	6.414	-0.034	95.0	6.400	6.408	-0.13
85.0	6.412	6.411	+0.013	110.0	6.399	6.407	-0.13
105.0	6.410	6.407	+0.049	135.0	6.399	6.406	-0.11
125.0	6.406	6.404	+0.028	150.0	6.399	6.405	-0.10
140.0	6.405	6.402	+0.040	170.0	6.398	6.405	-0.11
165.0	6.405	6.400	+0.082	200.0	6.398	6.403	-0.081
190.0	6.405	6.397	+0.120	230.0	6.397	6.401	-0.068
210.0	6.405	6.395	+0.150	260.0	6.397	6.399	-0.028
220.0	6.399	6.395	+0.065	290.0	6.396	6.396	+0.003
230.0	6.398	6.394	+0.066	350.0	6.395	6.392	+0.11
240.0	6.393	6.393	+0.004	410.0	6.394	6.378	+0.24
260.0	6.387	6.391	-0.066	445.0	6.392	6.372	+0.31
280.0	6.381	6.389	-0.120	480.0	6.382	6.367	+0.23
310.0	6.375	6.384	-0.140	515.0	6.376	6.361	+0.23
340.0	6.371	6.378	-0.120	540.0	6.372	6.356	+0.24
370.0	6.370	6.371	-0.022	575.0	6.368	6.350	+0.29

* Calculations for E16 were based on the parameter values determined from E09b.

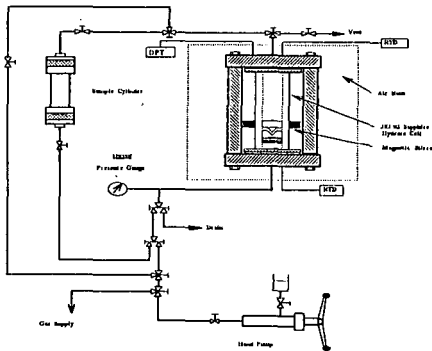


Fig. 1: Schematic diagram of the experimental system
 DPT—differential pressure transducer
 RTD—resistance thermocouple detector

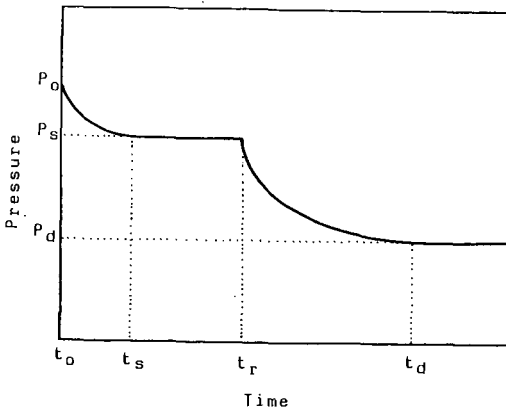


Fig. 2. A typical $P \sim t$ curve measured in this study

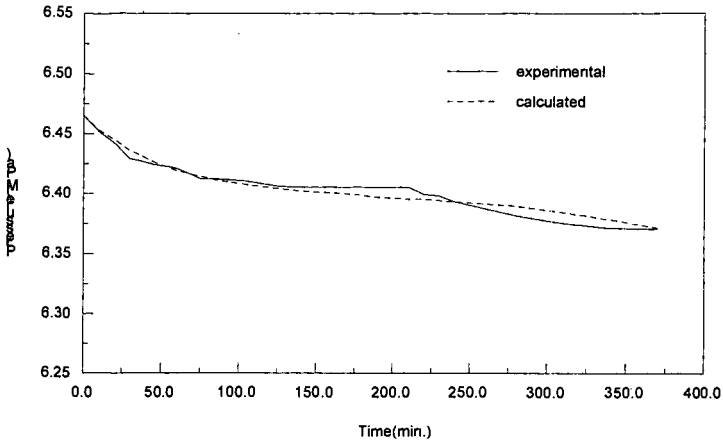


Fig. 3. The experimental and calculated $P \sim t$ curve for Experiment E09b

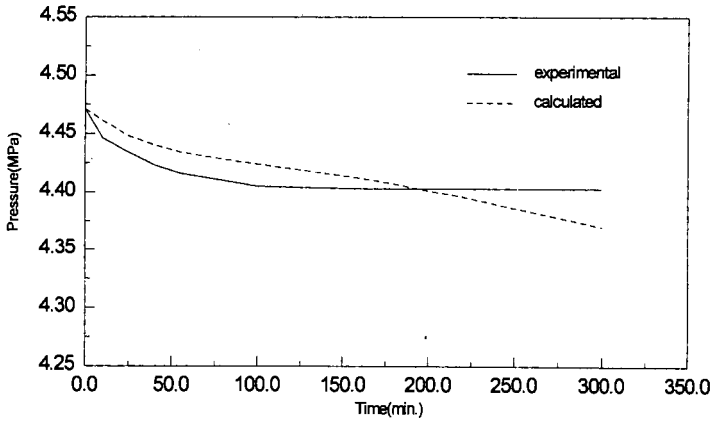


Fig. 4. The experimental and calculated $P \sim t$ curve for Experiment E01 (calculation based on the parameters determined for E04)

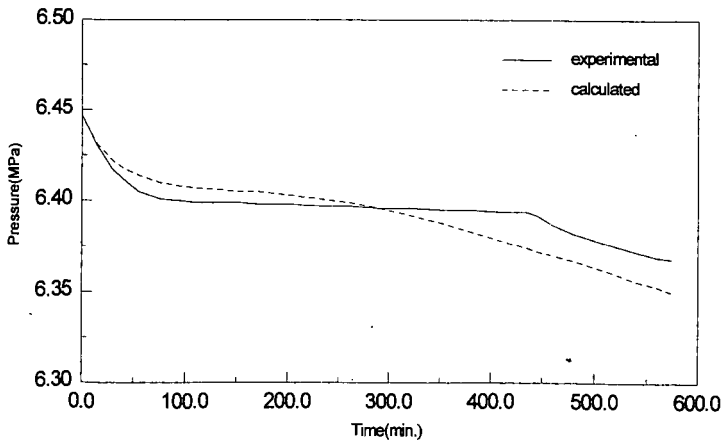


Fig. 5. The experimental and calculated $P \sim t$ curve for Experiment E16 (calculation based on the parameters determined for E09b)